Towards minimal perturbations in transitional plane Couette flow

Yohann Duguet, Luca Brandt, and B. Robin J. Larsson

Linné Flow Centre, KTH Mekanik, Osquars Backe 18, SE-10044 Stockholm, Sweden

For parallel shear flows, transition to turbulence occurs only for perturbations of sufficiently large amplitude. It is therefore relevant to study the shape, amplitude, and dynamics of the least energetic initial disturbances leading to transition. We suggest a numerical approach to find such minimal perturbations, applied here to the case of plane Couette flow. The optimization method seeks such perturbations at initial time as a linear combination of a finite number of linear optimal modes. The energy threshold of the minimal perturbation for a Reynolds number Re=400 is only 2% less than for a pair of symmetric oblique waves. The associated transition scenario shows a long transient approach to a steady state solution with special symmetries. Modal analysis shows how the oblique-wave mechanism can be optimized by the addition of other oblique modes breaking the flow symmetry and whose nonlinear interaction generates spectral components of the edge state. The Re dependence of energy thresholds is revisited, with evidence for a $O(\mathrm{Re}^{-2})$-scaling for both oblique waves and streamwise vortices scenarios.

PACS number(s): 47.27.Cn, 47.20.Ft

I. INTRODUCTION

Subcritical transition to turbulence can occur in a variety of wall-bounded shear flows when the laminar base state is not subject to linear instability [1]. Transition is often undesired in applications because it leads to a dramatic increase of the wall shear stress, and the total drag. Hence it is important to know which kind of (weak) perturbations is susceptible to trigger transition if one wishes to delay or control it. In a subcritical case, perturbations to the base state, with a finite but very small amplitude, can be amplified by non-normal effects, up to a level where nonlinear effects come into play. A vast amount of literature has described the linear mechanisms responsible for such an amplification in plane shear flows (see for instance Ref. [1] and references therein). Computational optimization methods can provide *linear optimal disturbances* [2,3], the initial disturbances which exhibit the largest possible transient energy growth. Linear amplification of such disturbances leads to spanwise modulations of the streamwise velocity, also called streaks. The resulting unsteady flow can support the transient growth of secondary optimal perturbations, and hence become fully three-dimensional [4,5]. An alternative approach to determine an optimal path to transition was recently suggested by Biau and Bottaro [6]. These authors sought perturbations eliciting a significant nonlinear response by considering the feedback of the fluctuations onto the mean flow. Yet the focus has been on linear amplification of the perturbation rather than on actual transition, which requires full nonlinearity to be taken into account. In this study, we go back to the original questions, namely: which kind of perturbation is most likely to trigger transition to turbulence? Through which physical mechanisms can transition occur with a least initial input of energy? We are hence investigating *nonlinear* optimal (or *minimal*) disturbances, those with smallest initial energy leading to a turbulence state.

The laminar base state is usually an analytically well-defined quantity, yet the notion of turbulent state is not. The latter is usually thought as an unsteady state of the fluid,

necessarily three-dimensional, where the amplitude associated with all wave numbers vary chaotically in time. Some recent studies suggested that turbulence in subcritical shear flows is necessarily transient, i.e., that the laminar state is the only globally attracting state in the system [7,8]. This is not supported by experimental investigation except for the lowest values of the Reynolds number where a turbulent flow can be triggered. Though quantitatively irrelevant at high Reynolds numbers, a nonzero probability for relaminarization prevents one from defining the turbulent state formally as an asymptotical state. In any case, an alternative, more pragmatic, criterion to identify whether the system has reached the turbulent state (albeit only transiently) is based on the level of energy fluctuations around the base state. Both experimental and numerical experience allow one to distinguish unambiguously between 'turbulent' fluctuations, with a broadband spectrum and a statistical average kinetic energy level E_T, and the laminar state with vanishing fluctuation energy. The minimal perturbations sought here are expected to have an initial energy $E_M > 0$ and to reach $E_T \gg E_M$ in a finite time, regardless of whether the turbulent state is sustained forever or not.

In the recent years, progress in the understanding of subcritical transition was made using the nonlinear concept of "edge state," originating from dynamical systems theory. "Edge state" refers to the flow regime reached asymptotically by phase-space trajectories visiting neither the turbulent state nor the laminar state. It is approached by trajectories starting from initial perturbations of arbitrary shape, whose amplitude corresponds to the exact amplitude threshold for transition [9]. It is an unstable flow state, whose instability mediates whether the system will return to the laminar state or evolve toward the turbulent regime. In the general case, the edge state has an unsteady dynamics. Crucially, experience has shown that it is characterized by a perturbation energy E_Σ much lower that than the energy of the turbulent state, i.e., $0 < O(E_\Sigma) \ll O(E_T)$. Direct numerical simulation in minimal domains of plane Couette flow has suggested that the edge state reduces to one unstable solution, characterized by wavy streaks and streamwise rolls [10,11]. This solution hap-
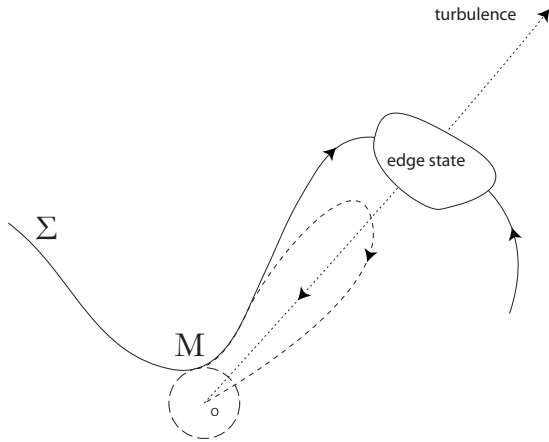
FIG. 1. Schematic view of the phase-space associated to the flow. Σ represents the laminar-turbulent boundary. O is the laminar state. The 'edge state' is the (unstable) asymptotical state on Σ. M is the minimal perturbation able to trigger transition to the turbulent state, i.e., the point on Σ closest to O in energy norm. Both the nonlinear (solid) and the linear (dashed) trajectories starting from M are shown here.

pens to be the steady state solution identified first by Nagata [12]. Under the assumption that this state is unique, the stable manifold of the equilibrium is of codimension one, and coincides with the laminar-turbulent boundary Σ (see Fig. 1). Yet more exact coherent states embedded in the edge state have also been identified numerically: traveling waves and relative periodic orbits in plane Couette flow [13], pipe flow [9,14–17], and plane channel flow [18–20], and the codimension of their stable manifolds is generally strictly larger than unity.

If actual transition is considered as undesirable, a *minimal perturbation* represents the most dangerous perturbation to the base flow. By construction, lowering the initial amplitude of this state would make the flow return to the laminar state, while amplifying its amplitude would cause transition. Hence such a state corresponds in phase space to a point M on the laminar-turbulent boundary Σ, located at a minimal distance from the laminar state with respect to the energy norm. Note that M is neither the asymptotical edge state nor one of the exact coherent states located on Σ. However, a trajectory starting from the neighborhood of M is expected to visit transiently the edge state, and this property allows one to greatly simplify the search for M: instead of looking for a trajectory reaching an energy level $O(E_T)$ in a finite time, we look explicitly for trajectories reaching $O(E_\Sigma)$ in an even shorter time. The nontrivial steady states of the system (which are nonlinear fixed points within a finite distance to the origin), can be seen as ideal targets for the trajectory starting from M. In the case where the edge state reduces to one single steady state, targeting its neighborhood in a finite time horizon represents an unambiguous dynamical constraint for the trajectory starting from M. Finding a trajectory hitting one of the (many) nontrivial solutions individually can however prove difficult using standard shooting methods because of their several unstable directions. Focusing on a traveling wave with unstable dimension two in cylindrical pipe flow, Viswanath and Cvitanović have demonstrated the

feasibility of finding trajectories approaching its immediate neighborhood in a finite time $T>0$ [21]. The method demands precise knowledge of the target state: the corresponding starting point at $t=0$ is a carefully optimized combination of streamwise rolls (extracted from the TW solution of interest) and the two unstable eigenvectors, all superimposed on the laminar base flow. In our investigation in turn, the energy of the perturbation at $t=0$ has to be minimized, rather than the passing-by distance to any of those exact states at a later time. Taking into account the usually complicated dynamics of the edge state as well as our lack of *a priori* knowledge of the embedded solutions, we only demand from the trajectory starting from M that it lie on Σ. Targeting the neighborhood of a steady state in a finite time horizon must not be seen as a generic case, and an ideal optimization method requires a dynamical target able to take into account an edge state with complicated dynamics. We will hence make pragmatic use of the criterion $0 < O(E_\Sigma) \ll O(E_T)$, and define *edge trajectories* as phase-space trajectories whose perturbation energy stays bounded at an asymptotic energy level $O(E_\Sigma)$ without ever visiting the turbulent state. Such ideal trajectories evolve on the laminar-turbulent boundary Σ, never to depart from it. With these definitions in mind, our quantitative objective is to find the edge trajectories with the smallest perturbation energy at initial time.

However, the dimension of Σ is supposed to be infinite, thus finding M is equivalent to solving an optimization problem in an infinite-dimensional space. In order to keep computations feasible, we need to consider a reduced optimization problem in a relevant finite-dimensional space of modest size m. It is natural to expect that the perturbation energy E_M associated with M is low enough for the dynamics in the neighborhood of M to be well approximated by linearized dynamics in the first stage of transition [22]. This would imply initial transient growth of the energy before it is progressively ruled by nonlinear dynamics. Since the target (the edge state) has energy $O(E_\Sigma)$, minimizing E_M is equivalent to maximizing E_Σ/E_M, i.e., the energy gain. The linearly most optimal modes are thus a natural candidate for a basis of the reduced space. We choose here to consider the initial perturbation of the problem as the sum of m low-order linearly optimal modes of given wave vector $\vec{\kappa}$ with suitably chosen complex coefficients $A_1, \ldots, A_m$. Minimizing the initial energy thus corresponds in practice to a search for optimal coefficients $A_i, i = 1, \ldots, m$. As we shall see, $m=2$ or 3 leads to an already costly numerical procedure, yet the associated results reveal the physically decisive trends, reconciling in passing the linear and nonlinear approaches to transition once meant to contradict each other [23,24]. Low values of m may not allow one to find the ultimate minimal perturbation accurately, however tracking the minimal state as m increases allows one to identify the physical mechanisms at play in the optimization. Note that our approach is however fully nonlinear, i.e., despite the use of linear modes in our expansion we never assume linearized dynamics in our computations.

We decide to test the optimization procedure in the context of plane Couette flow since it is the simplest example of subcritical shear flow. It should nevertheless be kept in mind that the formulation introduced here applies to any parallel

shear flow with a linearly stable laminar profile. The plan of the paper is as follows. Section II details the mathematical formulation of our approach, while the numerical tools used are described in Sec. III. Section IV presents the optimization results in $m=2$ and $m=3$ subspaces, in the case of plane Couette flow at Re=400. The whole transition scenario starting from the most efficient perturbation M is analyzed in spectral space, and the implications for further optimization are discussed. Several exact coherent states found during this investigation are also presented and discussed in relation with the literature. Finally, Sec. IV shows the asymptotic scaling of energy thresholds for the most efficient transition scenarios when increasing the Reynolds number.

II. MATHEMATICAL FORMULATION

A. Governing equations

Plane Couette flow is the incompressible flow between two countermoving parallel plates. The Reynolds number Re$=\frac{Uh}{\nu}$ is based on the plate velocities $\pm U$, the half-gap h and the kinematic viscosity ν. Length and time are expressed, respectively, in units of h and h/U while the mass density is set to unity. x, y, z stand, respectively, for the coordinates in the streamwise e_x, wall-normal e_y and spanwise e_z directions. The laminar base flow profile is $U_b=ye_x$. The velocity field of a perturbation to U_b reads $u=ue_x+ve_y+we_z$. it is governed by the Navier-Stokes equations in perturbative form,

$$\frac{\partial u}{\partial t} + (U_b \cdot \nabla)u + (u \cdot \nabla)U_b + (u \cdot \nabla)u = -\nabla p + \frac{1}{\text{Re}}\nabla^2 u,$$
(1)

$$\nabla \cdot u = 0,$$
(2)

where an initial perturbation u is prescribed at time $t=0$. It obeys the no-slip boundary conditions at the walls

$$u(y = \pm 1) = 0.$$
(3)

B. Reduction to a basis of linear optimal modes

We consider the state-space form associated with Eqs. (1) and (2) after spatial discretization,

$$\frac{dU}{dt} = LU + N(U), \quad U \in \Omega.$$
(4)

A state-space vector $U \in \Omega$ (respectively, V) is represented in physical space by an instantaneous three-dimensional velocity field for a perturbation $u(x,y,z)$ [respectively, $v(x,y,z)$] to the base flow. The associated scalar product is defined by

$$(U,V) = \frac{1}{V}\int u \cdot v^* dxdydz,$$
(5)

and the energy of a perturbation by $E = \frac{1}{2}(U,U)$, where V is a normalization constant denoting the volume of the computational domain. L is a stable but non-normal linear operator

$(L^*L \neq LL^*)$ and N represents the quadratic energy-conserving nonlinear terms. How the system (1) and (2) can be transformed into Eq. (4) can be found for instance in Ref. [22].

The time evolution of the energy is governed by the Reynolds-Orr equation,

$$\frac{dE}{dt} = (LU,U) + (N(U),U).$$
(6)

Because of the energy-conserving nature of the nonlinear terms, the term $[N(U),U]$ vanishes, and the potential amplification of the disturbance energy is fully contained in the linear term L [22]. Note that even if the rate of change of the total energy of a disturbance does not depend on its amplitude, the evolution of the associated three-dimensional velocity field does, as pointed out in Ref. [24].

By *minimal* or *nonlinear optimal* state, we mean the disturbance U of smallest initial energy leading to turbulence when advanced in time by the full nonlinear Eq. (4). We call Σ the laminar-turbulent boundary, i.e., the set of initial conditions in Ω evolving neither toward turbulence nor toward the laminar state. The reader is invited to refer to Sec. I for a discussion of how Σ is defined in case the turbulent state is not an asymptotic attractor. The search for the globally minimal state M is equivalent to seeking a state on Σ minimizing the perturbation energy E, i.e.,

$$E(M) = \min_{U \in \Sigma} E(U).$$
(7)

If the trajectory starting at M converges asymptotically to an edge state, the energy of M is, within the energy norm, a measure of the diameter of the basin of attraction of the laminar state. Note that $E(U)$ can also have local minima on Σ which are not global minima.

Two necessary properties of a minimal state [25] at the initial time are

$$\frac{dE}{dt} = 0 \Rightarrow (LU,U) = 0,$$
(8)

$$\frac{d^2E}{dt^2} > 0.$$
(9)

Condition (8) is independent of the amplitude of the perturbation and solely determined by the nature of the linear operator, since for any complex number λ, we have

$$[L(\lambda U),(\lambda U)] = |\lambda|^2(LU,U).$$
(10)

This implies that properties (8) and (9) are invariant under rescaling or phase shift of the perturbation. This is crucial for the bisection algorithm described later to find thresholds. Note that only the non-normality of the stable operator L allows for the existence of nontrivial solutions of Eq. (8). In order to find such solutions, we split the state space Ω in orthogonal subspaces all stable by the action of L. This can formally be written as the direct sum,

$$\Omega = \bigoplus_i E_i,$$
(11)

where

$$\forall \mathbf{U} \in E_i, \quad \forall \mathbf{V} \in E_{i'}, \quad i \neq i' \Rightarrow (\mathbf{U}, \mathbf{V}) = 0 \quad (12)$$

and

$$\mathbf{U} \in E_i \Rightarrow L\mathbf{U} \in E_i. \quad (13)$$

Now suppose that in *each* of these orthogonal subspaces we know one solution $\bar{\mathbf{U}}_i$ satisfying Eq. (8), then all the $\bar{\mathbf{U}}_i$'s span a whole linear space of states which all satisfy Eq. (8). For instance, using only two such subspaces, for $\bar{\mathbf{U}}_i \in E_i$, $\bar{\mathbf{U}}_j \in E_j$, and $i \neq j$,

$$[L(\bar{\mathbf{U}}_i + \bar{\mathbf{U}}_j), (\bar{\mathbf{U}}_i + \bar{\mathbf{U}}_j)] = \cancel{(L\bar{\mathbf{U}}_i, \bar{\mathbf{U}}_i)} + \cancel{(L\bar{\mathbf{U}}_j, \bar{\mathbf{U}}_j)} \quad (14)$$

$$+ \cancel{(L\bar{\mathbf{U}}_i, \bar{\mathbf{U}}_j)} + \cancel{(L\bar{\mathbf{U}}_j, \bar{\mathbf{U}}_i)} \quad (15)$$

$$= 0. \quad (16)$$

As for the orthogonal decomposition of Ω, we choose the subspaces spanned by Fourier harmonics $e^{i(\alpha k_x x + \beta k_z z)}$, parametrized by two integers k_x and k_z. These modes are stable by the action of the operator L because the base flow is parallel and depends only on the wall-normal coordinate y. In each subspace $E_{(k_x, k_z)}$, there is at least one perturbation satisfying Eq. (8), namely, the *linear optimal mode* yielding the largest possible amplification over all final times. For a given (k_x, k_z), the global optimal $\bar{\mathbf{U}} \in E_{(k_x, k_z)}$ maximizes the linear energy gain G_L over all times. It is defined by:

$$G_L = \max_{\mathbf{U}, t} \frac{(e^{tL}\mathbf{U}, e^{tL}\mathbf{U})}{(\mathbf{U}, \mathbf{U})}. \quad (17)$$

Each mode $\bar{\mathbf{U}}$ results in physical space from an optimization over both time and its y-profile. From a state-space perspective, it results from the singular-value decomposition of the matrices e^{tL}, later to be optimized over different times t [3].

The search for a globally minimal state over the full phase-space remains quite ambitious, and we want to exploit the decomposition [Eq. (11)] to look for local nonlinear optima in relevant subspaces where expressions (8) and (9) are satisfied. Let us choose a finite number of linear optimal modes $\bar{\mathbf{U}}_1, \ldots, \bar{\mathbf{U}}_m$, each corresponding to different harmonics in x and z, and a vector of complex amplitudes $\mathbf{A} = (A_1, \ldots, A_m)$. We can formally build any linear combination

$$\mathbf{U}_A = \sum_{i=1}^{m} A_i \bar{\mathbf{U}}_i. \quad (18)$$

If by rescaling the amplitude of $\mathbf{U}_A$, the system can undergo transition to turbulence, then it is possible to define a critical threshold energy noted E_c associated with each vector $\mathbf{A}$ (see Sec. III B). The linear optimal modes $\bar{\mathbf{U}}_i, i = 1, \ldots, m$ span a finite complex-valued space of dimension m with its own laminar-turbulent boundary Σ_m. In the reduced subspace, the search for minimal states becomes the optimization problem,

$$\min_{\mathbf{A} \in \mathbb{C}^m} \{E_c, \mathbf{U}_A \in \Sigma_m\}. \quad (19)$$

To make the problem yet tractable, a choice of the subspaces $i = 1, \ldots, m$ must be made, with m being as small as possible. The first effective reduction is to only retain the lowest-order harmonics in x and z. We therefore decided to test these ideas by using only modes corresponding to $|k_x| \leq 2$ and $|k_z| \leq 2$. This is justified by the poor amplification gain associated with higher-order harmonics, which would not contribute much to the growth of the most efficient perturbations.

III. NUMERICAL METHODS

A. Direct numerical simulation

The numerical code (see Ref. [26] for details) is based on an expansion of the three-dimensional velocity perturbations on Fourier modes in x and z, and Chebyshev polynomials in y,

$$\mathbf{u}(x, y, z, t) = \sum_{m=0}^{M} \sum_{k_x=-L}^{L} \sum_{k_z=0}^{K} \widehat{\mathbf{u}}_{k_x, k_z, m} e^{i(\alpha k_x x + \beta k_z z)} T_m(y). \quad (20)$$

This spectral formulation can be associated with an autonomous dynamical system in a phase-space $\Omega \cong \mathbb{R}^n$, where $n = O(2KLM)$. A fourth-order Runge-Kutta algorithm is used to advance Eq. (1) in time. The time step has order of magnitude $O(10^{-2})\frac{h}{U}$. The boundary conditions are periodicity in x and z, and no-slip at the walls ($y = \pm 1$). $L_x = \frac{2\pi}{\alpha}$ and $L_z = \frac{2\pi}{\beta}$ are, respectively, the streamwise and spanwise dimensions of the domain. In this study $L_z = 2\pi$ and $L_x = 4\pi$, as in Ref. [11], except in Sec. IV E where L_x is varied. Note that $L_z = 2\pi$ corresponds to the typical wavelength of two pairs of streamwise streaks. The value of Re used for most of the computations is 400, and it is increased up to 3500 in Sec. V. The numerical resolution consists of 48 collocation points in x, 33 in y and 48 in z, ensuring a drop of 10 decades in the energy spectrum near the edge state. This corresponds to a phase-space of dimension $n \sim 1.5 \times 10^5$. For Re above 1500, it proved necessary to increase the resolution to 65 in y and 64 in x and z.

Continuation in Re of the steady state solutions found during this investigation was made using a Newton-Krylov algorithm in the full space $\mathbb{R}^n$. The algorithm is essentially the same as in Ref. [17], adapted to the search for steady solutions. The use of the Double Dogleg globalisation technique allowed for very large Re steps. The criterion used for convergence to each of these solutions is $|\mathbf{U}(t=T) - \mathbf{U}(t=0)|_2 = O(10^{-11})$ with $T = 15$, where $|.|_2$ stands for the Euclidian norm in $\mathbb{R}^n$.

B. Determination of threshold energy for transition

Let $\mathbf{U}_0$ be any given perturbation to the base flow, γ a real positive number, and suppose that the initial condition is $\gamma \mathbf{U}_0$. Because the base flow is linearly stable, the system is expected to transit to turbulence for γ large enough (possibly infinite), while it relaminarizes for γ small enough. In all
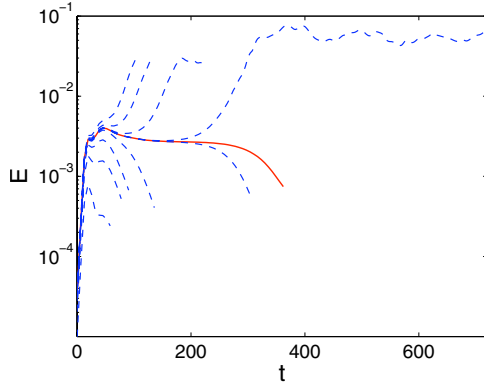
FIG. 2. (Color online) Bisection algorithm. Kinetic energy of the perturbation velocity versus time when varying the initial amplitude. The initial condition whose evolution is indicated by the red solid line corresponds to the minimal perturbation M described in the text consisting of the three linearly optimal modes $(k_x, k_z) = (1, \pm 1)$ and $(1,2)$.

cases where transition to turbulence does occur, we use a standard bisection on γ to seek a value $\gamma = \gamma_c$ such that the trajectory starting from $\gamma_c U_0$ stays on Σ, i.e., neither relaminarizes nor becomes turbulent [9,11,16,20]. As discussed in Sec. I, the method relies on an unambiguous distinction between energy levels of the perturbation on the edge and in the turbulent regime, i.e., $O(E_\Sigma) \ll O(E_T)$ [typically, $E_T \sim O(10^{-1})$ and $E_\Sigma \sim O(5 \times 10^{-3})$ for Re=400, see Fig. 2]. Note that it is not an issue whether the intersection between the line spanned by U_0 and Σ is uniquely defined or not (for instance if Σ is multiply folded), as the bisection algorithm returns one initial condition which is on Σ anyway. With each perturbation U_0 able to trigger turbulence ($\gamma_c < +\infty$), we can hence associate a critical energy E_c, which is the energy of the perturbation $\gamma_c U_0$. Numerically, γ_c can be determined down to machine precision $\delta\gamma_c \sim O(10^{-15})$ though for our purpose $\delta\gamma_c \sim O(10^{-10})$ proved sufficient.

C. Optimisation procedure

Since the amplitudes $A_i, i=1, \ldots, m$ of the optimal modes are complex numbers, choosing m modes for the ansatz in Eq. (18) implies $2m$ real degrees of freedom. This can actually be reduced down to $l = 2(m-1) - 1$. In the definition of l, the substitution $2m \leftarrow 2(m-1)$ is due to the normalization of the amplitude of the first mode to (complex) unity, since we seek only the shape of the initial perturbation and can deduce the critical amplitude *a posteriori*. The final reduction $l \leftarrow l-1$ comes from the fact that the results are independent of the phase of mode 2 because the base flow is homogeneous in x and z. In the following we will gather the new real coefficients to be found in a vector $\Lambda = (\lambda_1, \ldots, \lambda_l)$.

The bisection method described in Sec. III B allows one to define a scalar function E_c acting on $\mathbb{R}^l$,

$$E_c : \Lambda = (\lambda_1, \ldots, \lambda_l) \to E_c. \tag{21}$$

A minimal perturbation is necessarily a local minimum of E_c, i.e.,

$$\mathbf{g} = \mathbf{0}, \tag{22}$$

where $\mathbf{g}$ is the gradient of E_c evaluated for a given l-dimensional vector Λ. The l components of the $\mathbf{g}$ are given, respectively, by

$$\mathbf{g}_i = \frac{\partial E_c}{\partial \lambda_i}, \quad i = 1, \ldots, l. \tag{23}$$

A standard Newton-Raphson method is used to find iteratively sets of coefficients $\lambda_1, \ldots, \lambda_l$ yielding local minima of E_c. At each iteration k, the vector $\Lambda^{(k)}$ containing the amplitudes is updated by $\Lambda^{(k+1)} = \Lambda^{(k)} + \delta\Lambda^{(k)}$. The increment $\delta\Lambda^{(k)}$ is found by solving the $l \times l$ linear system,

$$\mathbf{H}^{(k)} \delta\Lambda^{(k)} = -\mathbf{g}^{(k)}. \tag{24}$$

In Eq. (24), $\mathbf{H}^{(k)}$ is the $l \times l$ Hessian matrix associated to E_c and evaluated at $\Lambda^{(k)}$. Its components are given by

$$(\mathbf{H}^{(k)})_{ij} = \frac{\partial \mathbf{g}_i}{\partial \lambda_j}. \tag{25}$$

All components of the vector $\mathbf{g}$ and the matrix $\mathbf{H}$ are evaluated numerically using standard first-order finite differences with a step ϵ,

$$g_i^{(k)} = \frac{E_c(\Lambda^{(k)} + \epsilon \mathbf{e}_i) - E_c(\Lambda^{(k)})}{\epsilon}, \tag{26}$$

$$(\mathbf{H}^{(k)})_{ij} = \frac{g_i(\Lambda^{(k)} + \epsilon \mathbf{e}_j) - g_i(\Lambda^{(k)})}{\epsilon}, \tag{27}$$

where $\mathbf{e}_i, i=1, \ldots, l$ stands for the unit vector in the ith direction.

The step ϵ has to be larger than the accuracy $O(\delta\gamma_c)$ of the bisection algorithm (determining the accuracy of E_c) but must remain small compared to the amplitude of the components of λ, which reads $O(\delta\gamma_c) \ll \epsilon \ll O(\Lambda)$. This is fulfilled in practice by choosing $\epsilon = 10^{-7}$. Convergence toward a local minimum is decided based on the criterion $|\mathbf{g}^{(k)}|_2 = O(10^{-4})$. Exploiting the symmetries of $\mathbf{H}$, the full algorithm amounts to $O(l^2/2)$ evaluations of E_c per Newton step. Note that the computational cost of each evaluation of E_c is the practical limitation of the method. Typically between 25 and 35 time integrations of the governing equations were necessary for the bisection algorithm to determine the threshold energy for transition. These types of simulations were performed for three different transition scenarios: two involving streaks and oblique waves and one for the pure oblique scenario. Threshold for transition were sought using 2 and 3 initial modes. Note also that preliminary simulations were performed using streaks of different size as well as two-dimensional modes. These yielded large threshold energies and are therefore not reported. More than 50 attempts were carried out to determine the minimal M presented here. Quasi-Newton methods, like the Broyden algorithm, use only $O(l)$ evaluations of E_c, but did not provide faster convergence for the values of l tested here.
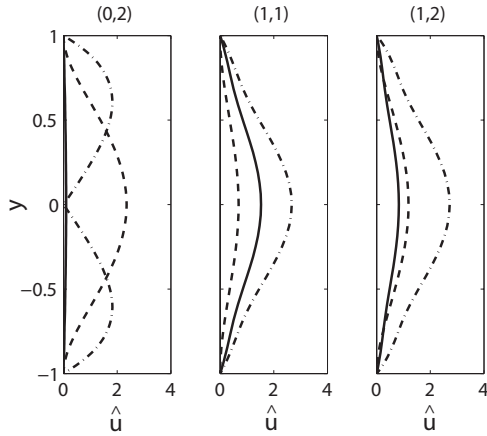
FIG. 3. Absolute value of the wall-normal profile of the Fourier modes $\hat{u}(y)_{k_x,k_z}$ for three of the linearly optimal modes considered in the optimization procedure. (SV): $(k_x, k_z) = (0, 2)$, $G_L(t = 48.5) = 176$; (OW): $(k_x, k_z) = (1, 1)$, $G_L(t = 19.4) = 85.5$ and $(k_x, k_z) = (1, 2)$, $G_L(t = 18.3) = 108.6$. Streamwise velocity: solid line. Wall-normal velocity: dashed line. Spanwise velocity: dash-dotted line.

IV. RESULTS

A. Streamwise vortices (SV) and oblique waves (OW) scenarios

The linearly optimal modes used in this study will be classified according to the pair of integers (k_x, k_z). The analysis will focus on two different transition scenarios both associated with the generation of streamwise streaks and their subsequent secondary instability. Wall-normal profiles of three of the modes used are displayed in Fig. 3 with the corresponding energy gain G_L reported in the caption. First, we consider the optimal modes associated with the largest linear amplification. They correspond to *pure streamwise vortices* (SV) with $k_x = 0$ and no initial streamwise velocity [1,2]. During the transient growth phase in the linear regime, energy is transferred to the streamwise velocity component via the lift-up effect creating low-speed and high-speed streamwise streaks. However, in the nonlinear regime, a mode $(0, k_z)$ alone cannot trigger transition to turbulence as no energy is transferred to streamwise-dependent modes. Transition through the SV scenario will hence necessarily need the addition of another mode with $k_x \neq 0$, e.g., $(1,1)$ or $(1,2)$. In this study where $L_z = 2\pi$, we will focus mainly on the mode with $k_z = 2$ which corresponds to a transition path characterized by the breakdown of two pairs of streamwise vortices as observed in Ref. [11]. The study of this transition path is also motivated by the procedure to compute nonlinear solutions in various shear flows used in Refs. [15,18].

The second scenario is based on the generation of the dominant streamwise-independent perturbations by nonlinear interactions of modes with $k_x \neq 0$. In particular, we consider at time $t = 0$ the presence of two symmetric oblique waves, $(1,1)$ and $(1,-1)$ (see Fig. 3), whose interaction again forces the $(0,2)$ mode. This scenario has been previously investigated by Schmid and Henningson [27] and requires lower levels of the initial energy in Ref. [28]. This transition path

will be referred to as *pure oblique-wave scenario* (OW). Note that OW perturbations belong to a symmetry subspace stable by integration in time of the Navier-Stokes equations, thus the final turbulent state verifies those symmetries as well. In order to illustrate this, it is enough to note that all modes excited by nonlinear interactions of $(1,1)$ and $(1,-1)$ necessarily read $(a+b, a-b)$, where a and b are integers. This property appears to be generic for plane parallel shear flows, since only nonlinearity is able to couple different wave numbers in x and z. The set of those modes cannot span the entire broadband spectrum typical of turbulent fluctuations, in the same way as a bishop on a chessboard stays on a same color throughout the whole game. The turbulent state triggered by OW perturbations in plane Couette flow hence corresponds to a special and nongeneric case of symmetric turbulence. The generation of a realistic (i.e., nonsymmetric) turbulent state necessitates the initial introduction of a third mode which does not form a triad with the modes $(1, \pm 1)$. This justifies *a priori* the need for an optimization in the $m = 3$ space.

B. Results of the optimization

A large number of preliminary computations of E_c for different combinations Λ was done in order to locate good initial guesses for the Newton algorithm, using all possible combinations of modes with $|k_x|, |k_z| \leq 2$ in Eq. (18).

1. $m = 2$ optimization

We start by describing the results of the optimization for $m = 2$ ($l = 1$) for which the computational cost of each Newton step stays moderate. For the case of two oblique modes $(1,1)$ and $(1,-1)$, a combination with equal initial amplitude is a locally optimal perturbation on Σ_2. The critical energy associated with this combination is $E_c^{OW} = 3.34 \times 10^{-5}$. As stated before, for the SV scenario, an optimal mode $(0,2)$ alone is unable to trigger transition. Thus we have added various three-dimensional oblique modes to obtain a finite threshold energy. A combination of the modes $(0,2)$ and $(1,2)$ was found to be optimal in the corresponding subspace Σ_2 when the ratio of the initial modal energies is $E_{(1,2)} = 0.0965E_{(0,2)}$, corresponding to a total threshold energy $E_c = 1.98 \times 10^{-4}$. When perturbing the $(0,2)$ mode with a $(1,1)$ mode, the optimal combination has a threshold energy $E_c = 1.72 \times 10^{-4}$ for a higher modal ratio $E_{(1,1)} = 0.485E_{(0,2)}$. In this case, the energy in the streak $(0,2)$ mode is 67% of the total initial energy of the perturbation. Other combinations yield larger values of E_c and will not be considered. The pure OW scenario thus appears to be more efficient than the streamwise scenario for $m = 2$, consistently with the conclusions in Ref. [28]. The corresponding threshold energy for the pure OW scenario at Re=400 is one decade below that of the SV scenario.

2. $m = 3$ optimization

We have tried to find trimodal combinations, with a threshold energy E_c hopefully below that for the classical scenarios associated with $m = 2$ and investigated earlier. Note that with the notations of Sec. III B, $m = 3$ complex ampli-
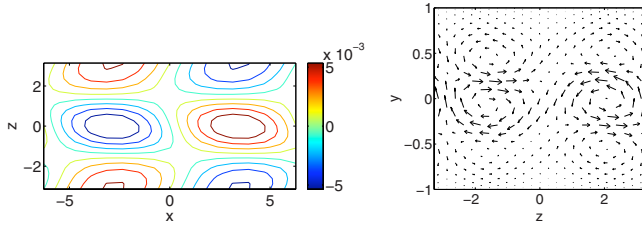
FIG. 4. (Color online) Initial condition of minimal energy leading to turbulence for $m=3$. The state is the superposition of three linearly optimal modes with wave number $(k_x,k_z)=(1,\pm 1)$ and $(1,2)$, where the complex amplitudes are determined by the optimization procedure. Streamwise velocity in the midplane $y=0$ (left), cross-stream velocity field in a section $x=0$ (right).

tudes corresponds to $l=3$ real degrees of freedom too. The optimization procedure is as follows: once three given modes $i=1,2,3$ have been chosen, the algorithm is run with $m=2$ using the first two modes, as a first guess for the order of magnitude of their amplitude. Later the third mode is added as a small perturbation (10% in amplitude) to the two other ones, with a varying phase. For each combination, ten different values for the phase were considered in order to build synthetic initial conditions. The Newton algorithm described in Sec. III C was run from (in total) 60 various initial conditions, representing altogether 500 days of CPU time. As we will see, convergence toward a local minimum of E_c is far from being guaranteed but has occurred once during the course of our investigation. Note first that attempts to design trimodal perturbations involving the SV mode $(0,2)$ have not showed any improvement of E_c compared to bimodal cases. Similarly, initial conditions including the modes $(1,1)$ and $(1,-1)$ with equal amplitudes, as well as another third mode, have not lead to better values of E_c either. Fixing the ratio $\lambda^{(1,1)}/\lambda^{(1,-1)}$ to one in the Newton-Raphson algorithm (meaning in practice an optimization on two modes only) lead to a very small improvement of E_c. Initial conditions including the modes $(1,1)$ and $(1,-1)$ with free and unbalanced amplitudes, as well as another third mode, were investigated more extensively. Only one local minimum of E_c was identified using the Newton scheme. It occurs when perturbing two oblique modes $(1,1)$ and $(1,-1)$ by the oblique mode $(1,2)$. It is characterized by the real amplitude triplet $(\lambda^{(1,1)},\lambda^{(1,-1)},\lambda^{(1,2)})=(1.37\times10^{-3},1.05\times10^{-3},-1.9\times10^{-4})$. The associated value of E_c is 3.276×10^{-5}, thus only 2% less than E_c^{OW}. The state corresponding to this minimal perturbation is now referred to as M throughout the paper. The associated velocity field is depicted in Fig. 4.

C. Transition scenario starting from the minimal perturbation with $m=3$

In this subsection we consider the minimal perturbation M found previously as a result of the Newton-based optimization. In principle, if M is determined with infinite accuracy, it belongs to Σ, itself invariant by the flow. However, for any $\hat\varepsilon>0$ sufficiently small, the trajectory starting from the perturbation M with a prefactor $(1+\hat\varepsilon)$ in its amplitude spends only a finite time in the immediate neighborhood of Σ before
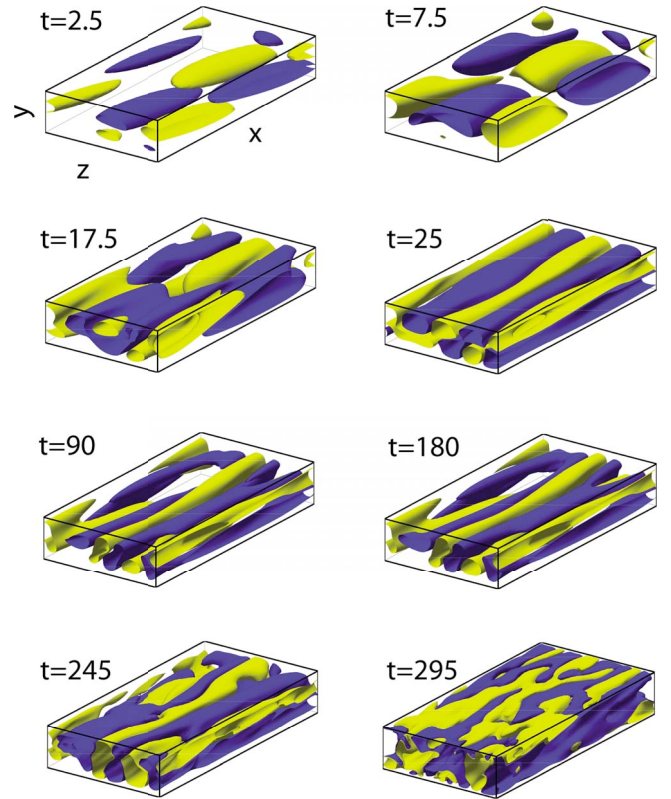

FIG. 5. (Color online) Three-dimensional view of the time evolution of the wall-normal velocity, $v=\pm 4\times10^{-3}$, along the trajectory T_{opt} initiated by the minimal perturbation M with amplitude $(1+\hat\varepsilon)$ (see text). From top to bottom and from left to right, $t=2.5,7.5,17.5,25,90,180,245,295$.

moving to another region of phase-space associated with turbulence. We consider such a phase-space trajectory near the threshold and denote it by T_{opt}. T_{opt} is actually a by-product of the bisection algorithm [when $\delta\gamma_c=O(\hat\varepsilon)$]. In Fig. 5, we show various three-dimensional snapshots of the wall-normal velocity field v. From $t=0$ to $t=10$, the oblique-wave pattern gets strongly distorted by the shear. Its initially upward-tilted shape turns rapidly into a downward-tilted one, which reminds one of the linear Orr mechanism in shear flows [1]. This is associated with the linear transient growth of the oblique modes. After $t=10$, the structures elongate in the downstream direction and the disturbance is dominated from $t=20$ on by streamwise vortices with a small but noticeable streamwise undulation. After $t=40$, the dynamics slows down dramatically. Between $t=80$ and $t=220$, the spatial structure of the perturbation hardly changes; this phase corresponds to the transient approach toward a steady state solution which we call here $E1$. The duration of the transient approach increases with decreasing $\hat\varepsilon$. Near $t\sim240$, the low-speed streaks start to distort. The velocity field suddenly becomes very unsteady. By $t\sim270$ it has all the qualitative features of the turbulent flow reached at Re=400 from other initial disturbances: elongated streamwise structures, larger amplitude of the velocity fluctuations, stronger unsteadiness.

The energy contained in each Fourier mode of the perturbation was computed at each time. The most energetic contributions are plotted versus time in Fig. 6. At $t=0$ only the
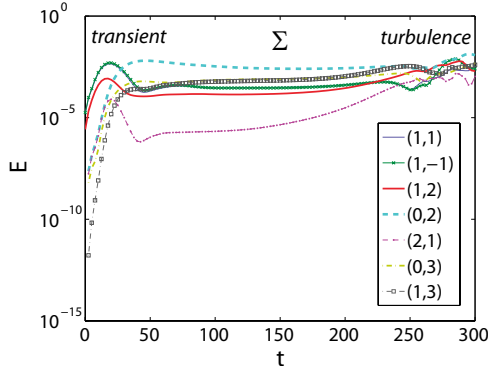
FIG. 6. (Color online) Time evolution of the energy E of several Fourier modes (k_x, k_z) (see legend) along the trajectory T_{opt}. The initial condition is the minimal perturbation M described in the text amplified by the factor $(1+\hat{\varepsilon})$.

modes $(1,1)$, $(1,-1)$, and $(1,2)$ are present, by construction, with the amplitudes given by the Newton algorithm. A few time steps later, all Fourier modes (k_x, k_z) with $|k| \leq 2$ are excited in the flow and start to grow quickly in energy, the $(0,2)$ streaky mode emerging faster. One order in magnitude below one detects higher-order modes, for instance the mode $(1,3)$ visible in Fig. 6. Their growth is by several decades larger than their maximum linear gain G_L. This shows that those modes are continuously fed by the driving modes and that their growth results from *nonlinear* interactions, present from $t=0$ onward. The $(1, \pm 1)$ and $(1,2)$ modes also undergo a growth in energy; the magnitude of this amplification is of amplitude comparable to the linear gain G_L of the corresponding mode, which is of order $O(10^2)$ for Re$=400$. From Fig. 6 it is apparent that the $(0,2)$ mode dominates from $t=30$ onward, explaining the streamwise structures forming around $t=20$ and then growing (see Fig. 5). At $t=80$, all components have reached a steady plateau. The modal energies all stay constant until $t \sim 200$ after which they all start to grow in a seemingly exponential manner [with the exception of the mode $(2,1)$ whose plateau is of shorter duration and shows the instability of the edge state]. Above $t \sim 250$, the dynamics of the flow is clearly turbulent and is still dominated by the $(0,2)$ mode.

The nonlinear interactions occurring along T_{opt} are quadratic and can be expressed as a sum of the wave numbers $\pm (k_x^1, k_z^1) \pm (k_x^2, k_z^2) \rightarrow (\pm k_x^1 \pm k_x^2, \pm k_z^1 \pm k_z^2)$. Such obvious quadratic interactions are here for instance:

(i) $(1,1)-(1,-1) \rightarrow (0,2)$ (generation of streamwise vortices);

(ii) $(1,2)-(1,-1) \rightarrow (0,3)$;

(iii) $(1,2)+(1,-1) \rightarrow (2,1)$;

(iv) $(1,2)-(1,1) \rightarrow (0,1)$;

(v) $(1,2)+(1,-1) \rightarrow (2,1)$;

(vi) $(0,2)+(1,1) \rightarrow (1,3)$ (active later in time).

All the interactions mentioned above are evident in Fig. 6. The initial presence of the $(1,2)$ mode allows the generation of more harmonics, however the differences between the initial disturbance M and the case of pure OW [with initial energy in modes $(1,1)$ and $(1,-1)$ only] seems only quantitative: in both cases the $(0,2)$ mode, typical of both the edge state and the turbulent field, dominates. The qualitative pic-

ture associated with the trajectory T_{opt} is clear: while the three excited modes initially grow in a linear fashion, they continuously transfer energy to other modes through quadratic interactions. All modes approach transiently a plateau which corresponds to the steady state $E1$. The instability of $E1$ is illustrated by the exponential growth of some Fourier modes representative of the structure of the unstable eigenvectors of $E1$, i.e., $(2,1)$. Among the modes generated by nonlinear interaction with $(1,2)$, $(0,3)$ has a relatively large amplitude during the visit to $E1$, actually the largest after $(0,2)$ in Fig. 6. This mode $(0,3)$ cannot be triggered by direct quadratic interaction of $(1,1)$ and $(1,-1)$ only, whereas it is an important spectral component of the edge state $E1$; therefore the initial introduction of the mode $(1,2)$ allows to shortcut more complex interactions and to reach $E1$ more directly. This might explain why M is slightly more efficient than the pure OW scenario. However, this improvement is only of 2% in threshold energy and is hence weak. The modal analysis suggests that the mechanisms at play on T_{opt} are initially the same as those in the OW case: quadratic interaction and generation of new modes, among them streamwise vortices, followed by a lift-up process, the transient approach to $E1$ and its instability.

D. Steady state solutions

For most of the initial conditions tested on Σ_3, the edge trajectories computed when evaluating E_c either converged to steady state solutions or spent a very long time in their neighborhood. During this study we identified not one, but three different steady state solutions on Σ. Which one is visited depends on the shape and the symmetries of the initial perturbation. The steady states found in this investigation are depicted in Figs. 7 and 8, where the velocity field in planes parallel and normal to the walls is shown. They are here refined down to machine accuracy using the Newton-Krylov solver referred to in Sec. III A. The steady state denoted $E1$ has lower perturbation energy than the two others, denoted $E2$ and $E3$. $E1$ displays low-speed streaks with a varicose structure, see Fig. 7. This steady state is approached by edge trajectories starting from the neighborhood of M. This is the case for the trajectory T_{opt} considered in the previous subsection. If T_{opt} is recomputed with an even smaller value of $\hat{\varepsilon}$, then the approach to $E1$ is still long but only transient. Note that in the special case where the initial perturbation is a pair of oblique waves with equal amplitude, the edge trajectory seems to converge toward $E1$, never to depart from it. When the initial condition corresponds to perturbations of optimal streamwise vortices (see Sec. IV B 1), the edge trajectories converge toward to either of the two steady states $E2$ or $E3$. $E2$ is reached optimally by initial conditions consisting of streamwise rolls and a small amount of perturbation in the Fourier component $(1,2)$, of the order of few percents of the total energy. Conversely, the solution $E3$ is approached by a perturbation where the energy in the oblique mode $(1,1)$ is about half of that of the streamwise rolls. $E2$ has two wavy streamwise streaks with one sinuous oscillation within our computational box, see Fig. 8. It appears as the most likely to be visited, and we believe that it corre-
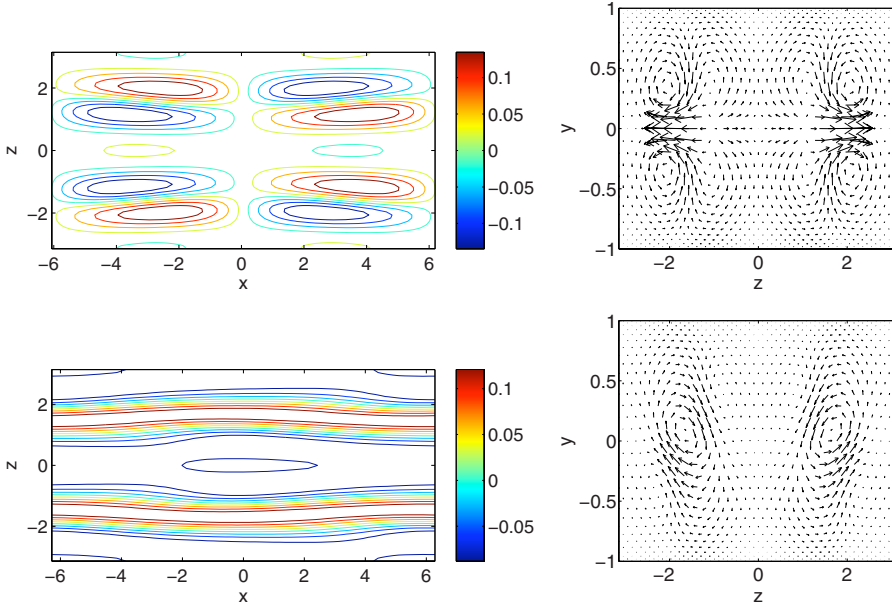
FIG. 7. (Color online) Steady state $E1$ approached by OW perturbations as well as by the optimal state M for $m=3$. Left: isocontours of the streamwise velocity field in the wall-parallel (x,z) plane at $y=0$ (top) and $y=0.4$ (bottom). Right: Cross-stream velocities in the cross-stream (y,z) plane at $x=0$ (top) and $x=-2.75$ (bottom).

sponds to the state identified in Ref. [12] and to the edge state found in Ref. [11]. $E3$, the most energetic among those found in our configuration, also has two streamwise streaks but with two streamwise oscillations. Bisection runs performed during the optimization process suggest that $E1$ has a smaller basin of attraction on Σ_3 than $E2$ and $E3$. The energy associated with the different steady states observed is reported in Table I. The minimal energy required to approach them is also compiled in the table.

Careful examination of the full velocity fields of $E1$, $E2$, and $E3$ (suitably shifted in the x and z directions) shows that they are symmetric with respect to various spatial symmetry subspaces. The prime symmetries of the steady state solution $E1$ are listed below.

$$g_1{:}[u,v,w](x,y,z) = [u,v,w](x + L_x/2, y, z + L_z/2), \quad (28)$$

$$g_2{:}[u,v,w](x,y,z) = [u,v,-w](x,y,-z), \quad (29)$$

$$g_3{:}[u,v,w](x,y,z) = [-u,-v,w](-x,-y,z), \quad (30)$$

as well as any combination of those symmetries. Pure OW perturbations also have the symmetry g_1, which explains why edge trajectories starting from such initial conditions visit $E1$. As stated earlier, robust convergence of the edge trajectory toward $E1$ is limited to the case of pure OW, i.e., perturbations invariant under g_1. This shows that $E1$ has only one unstable direction in the g_1-invariant subspace, but has at least one unstable eigenvector outside that subspace. This explains why E_1 was not identified in Ref. [11]. It also demonstrates that our optimization method works even if the target has a stable manifold of codimension strictly larger than unity.
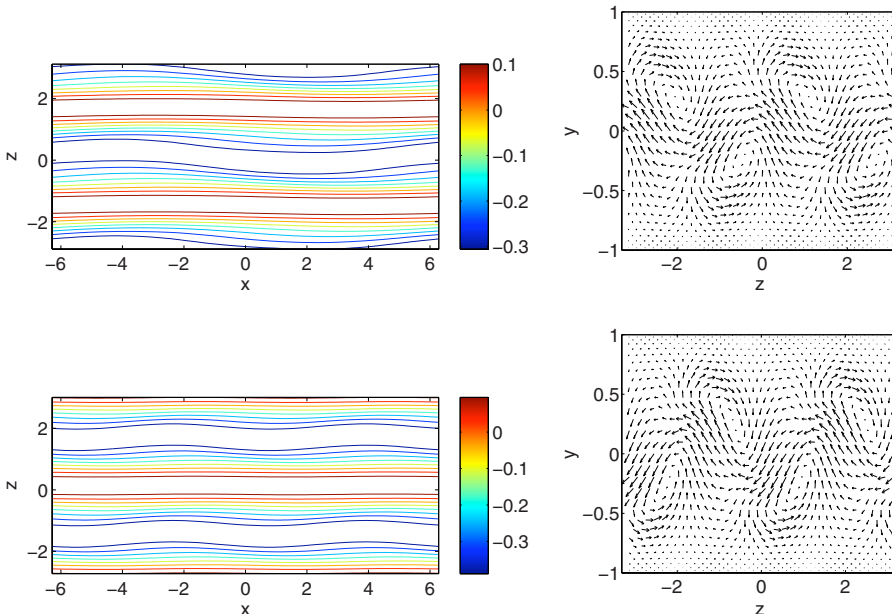

FIG. 8. (Color online) Steady states $E2$ and $E3$ approached by the different initial conditions corresponding to the SV scenario. From top to bottom, $E2$ and $E3$. Left: Cross-stream velocities in the cross-stream (y,z) plane at $x=0$. Right: iso-contours of the streamwise velocity field in the wall-parallel (x,z) plane at $y=0$.

TABLE I. Energy of the steady states identified with corresponding energy of the most efficient initial conditions able to approach them. The perturbation in the second line corresponds to the minimal perturbation M.

	Energy	Initial energy	Perturbation
$E1$	2.84×10^{-3}	3.34×10^{-5}	$E_{(1,1)} = E_{(1,-1)}$
$E1$	2.84×10^{-3}	3.276×10^{-5}	$E_{(1,2)} = 0.0192 E_{(1,1)} = 0.0327 E_{(1,-1)}$
$E2$	1.82×10^{-2}	1.98×10^{-4}	$E_{(1,2)} = 0.0965 E_{(0,2)}$
$E3$	2.61×10^{-2}	1.72×10^{-4}	$E_{(1,1)} = 0.48 E_{(0,2)}$

The steady state solution $E2$ and $E3$ have additional symmetries (apparent in Fig. 8): $E2$ and $E3$ have an axial wavelength $\lambda_z = L_z/2$ instead of the imposed wavelength Lz. $E3$ also has a spanwise wavelength $\lambda_x = L_x/2$ instead of L_x. Both states also obey the following prime symmetries:

$$s_1 : [u, v, w](x, y, z) = [u, v, -w](x + \lambda_x/2, y, -z), \quad (31)$$

$$s_2 : [u, v, w](x, y, z) = [-u, -v, w](-x, -y, -z + \lambda_z/2), \quad (32)$$

$$s_3 : [u, v, w](x, y, z) = [-u, -v, -w](-x + \lambda_x/2, -y, -z + \lambda_z/2), \quad (33)$$

Note that $s_3 = s_2 s_1 = s_1 s_2$, and that those symmetries form, along with the identity transformation, the isotropy group denoted S in Ref. [29]. The striking resemblance between the flow fields associated to $E2$ and $E3$ suggests the possibility that $E2$ can be traced back to $E3$ by homotopy in the parameter L_x.

The steady state solution $E1$ shares the symmetries of the lower-branch EQ7 solution of Ref. [29], also shown to be connected to the "hairpin vortex solution" of Ref. [30]. Visual inspection of the velocity fields *a priori* suggests a connection between $E1$ and the aforementioned solutions, despite the fact that the current computational domain ($L_x = 4\pi, L_z = 2\pi$) is much larger than the domain used in Ref. [29]. Note that $E1$, like EQ7, has lower kinetic energy than the other steady solutions identified so far on Σ. In order to shed some light on this resemblance, we have chosen to compute an edge trajectory for the same parameters as in Ref. [29]: $L_x = 5.51, L_z = 3.76, Re = 400$. The initial condition for the bisection chosen here is of OW type, i.e., a pair of symmetric oblique waves (like in Sec. IV B 1 but here with different wavelengths). The resulting edge trajectory has a chaotic dynamics but shows near $t \approx 100$ a relatively short transient approach toward the neighborhood of a state of constant energy. Visual inspection of the flow at $t = 100$ reveals a much stronger resemblance to the state EQ7 of Ref. [29], with the clear symmetric streak structure shared only, among all steady states known so far, by EQ7. This strongly suggests that EQ7 is embedded within the edge state for these parameters, even if rigorously speaking nothing prevents the coexistence of other similar steady solutions. Now we have already demonstrated in Table I that the steady state initially visited by the edge trajectory starting from
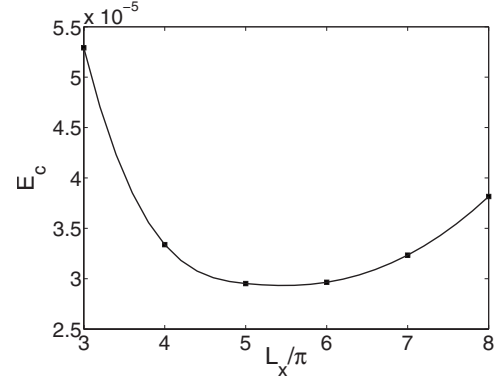

FIG. 9. Threshold energy E_c for transition initiated by a pair of symmetric oblique waves as a function of the streamwise length of the computational domain L_x scaled with π.

symmetric oblique waves with the parameters $L_x = 4\pi, L_z = 2\pi, Re = 400$ is the state $E1$. Using a continuity argument it is reasonable to believe that by smoothly changing the wavelengths L_x and L_z of the initial perturbation, the associated steady solution first visited on Σ will also change smoothly, provided the steady solutions of interest do exist along the chosen path in the (L_x, L_z) parameter space. This directly suggests that E1 ($L_x = 4\pi, L_z = 2\pi$) is connected to the hairpin vortex solution.

E. Dependence on the numerical domain for the OW scenario

The previous results clearly show that the minimal perturbations follow the oblique-wave scenario, with $E_c(M)$ only slightly different from E_c^{OW}. Hence instead of $E_c(M)$, we investigate how the critical energy for the pure oblique case E_c^{OW} depends on the wavelength L_x. Here we only consider even combinations of the two modes $(1,1)$ and $(1,-1)$ (themselves recomputed for different values of L_x) to calculate the threshold, after having checked that the modal distribution $E_{(1,1)} = E_{(1,-1)}$ is always optimal on Σ_2. Results are shown in Fig. 9 and indicate that the oblique wave leading to transition with the lowest energy density has an axial wavelength $L_x^{opt} = 5.5\pi$, associated with a threshold energy density $E_c^{opt} = 2.92 \times 10^{-5}$. This corresponds to an angle of $20°$ with respect to the streamwise direction. Note that the value of E_c^{opt} is quantitatively close to the optimal value found for $L_x = 4\pi$, which suggests that the results of the previous subsections can be safely used to draw conclusions about the nature of the optimal mechanism for transition.

V. ASYMPTOTIC BEHAVIOR

A. Threshold energies

We investigate the Re dependency of the threshold energy E_c corresponding to the two scenarios OW and SV, as well as the energy of the associated steady states visited on the edge. We focus on the case $L_x = 4\pi, L_z = 2\pi$ investigated earlier.

The energy thresholds for the OW scenario are obtained by considering only the modes $(1, \pm 1)$ with equal initial energy. As noted earlier, the turbulent state reached by OW perturbations belongs to a nongeneric symmetry subspace
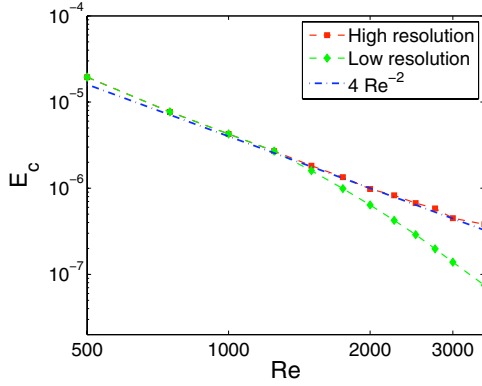
FIG. 10. (Color online) Threshold energy E_c for the pure oblique scenario as a function of the Reynolds number Re, for a computational domain of size $L_x = 4\pi$, $L_z = 2\pi$. The results obtained using low numerical resolution, similar to Ref. [28] (green diamond), are compared to well-resolved simulations where the number of grid points increases with Re (red square). The latter is well approximated by the function $4\,\mathrm{Re}^{-2}$ (dash-dotted line).

and does not represent a realistic turbulent field. However, the results of Sec. IV B have shown that the initial addition of a third mode at Re=400 leads to a broadband turbulent state with only a minor modification of the threshold energy E_c (less than 2%). Thus we disregard here the optimal scenario starting from M described earlier (whose continuation with Re is technically challenging) and focus instead on the pure OW mechanism. The steady solutions E_1, E_2, and E_3 identified during the transition process are computed for Re>400 by numerical continuation, starting from the solution at Re=400. Note that for the largest values of Re, the numerical resolution needs to be increased. Keeping the same resolution between Re=400 and Re=3500 leads to underestimated energy thresholds. We show evidence that the numerical thresholds computed in Ref. [28] suffer quantitatively from this lack of accuracy, and that the exponent predicted in that study, namely, −2.5 in energy, is overestimated. First we kept the numerical resolution of the low Reynolds number in Ref. [28] and used it to predict energy thresholds
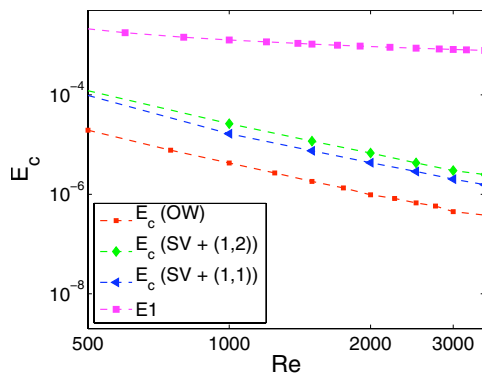

FIG. 11. (Color online) Comparison of threshold energy E_c versus the Reynolds number for the pure oblique-wave mechanism (red square), streamwise vortices (0,2) perturbed, respectively, by the (1,2) mode (green diamond) and by the (1,1) mode (blue triangle). The perturbation energy of the steady state $E1$, visited by oblique waves, is also indicated (large magenta square).

up to Re=3500. In this case we find the −2.5 exponent for Re ≈ 1500, which becomes −3 for Re ≈ 2000 and decreases further for even higher Re. When increasing the numerical resolution in all directions (especially in the wall-normal direction), a scaling closer to −2 emerges as shown Fig. 10.

Thresholds for the SV scenario were also analyzed as a function of Re. We have considered two different possible initial perturbations generated by adding to the streamwise-independent mode (0,2) either the oblique mode (1,1) or (1,2). In both cases, with careful care on the numerical resolution with increasing Re, we find an energy exponent of −2. This again corrects the value of −2.2 predicted by Reddy *et al.*, and fits the scaling suggested in Refs. [31,32]. The results shown in Fig. 11 shows a comparison between all threshold energies as a function of Re. It is apparent that both SV and OW scenarios lead to transition above a threshold energy of $O(\mathrm{Re}^{-2})$ $[O(\mathrm{Re}^{-1})$ in amplitude]. The energy threshold associated with oblique disturbances always stays one decade below that of streamwise vortices. The energy of the edge state $E1$ is also displayed in Fig. 11. As for $E2$ and $E3$, it tends asymptotically to a constant [10]. Note that the −2 threshold exponent for both OW and SV perturbations confirms the theoretical bound of $O(\mathrm{Re}^{-2})$ suggested by Chapman [31], as well as by Waleffe [32] in the case of the SV scenario. It might also be related to the experimental threshold amplitude $O(\mathrm{Re}^{-1})$ in pipe flow [33], though it is not clear yet how the definition of experimental disturbance amplitudes is related to the definition considered here.

B. Nonlinear amplification gain

We are now interested in extending the concept of linear transient growth to that of *nonlinear transient growth*. A proper definition of the *nonlinear gain* is needed and we suggest here two different definitions based on reproducible quantities, baptized, respectively, G_{NL}^e and G_{NL}^{os}. An important point is that, in order to describe transition to turbulence, only the dynamics of $E(t)$ *before* the approach to the edge state needs to be considered, and the final turbulent energy level E_T needs not be known. This is based on the idea that the dynamics *after* the edge state is controlled solely by the instability of the last steady state solution (belonging to Σ) visited by the diverging trajectory.

When the full nonlinear equations Eq. (1) are considered, it seems natural to define the *nonlinear gain* G_{NL}^e as the ratio between two energies: the energy of the first steady state S reached by the edge trajectory, and the initial energy at $t=0$,

$$G_{NL}^e = \frac{E(S)}{E(t=0)}. \qquad (34)$$

The superscript "e" in "G_{NL}^e" stands for "edge state." Clearly the energy $E(S)$ of the steady state has an order of magnitude $E(S) = O(E_\Sigma)$. Still, as in Ref. [3], we can define the linear gain G_L obtained by integration of the linearized perturbation equations as

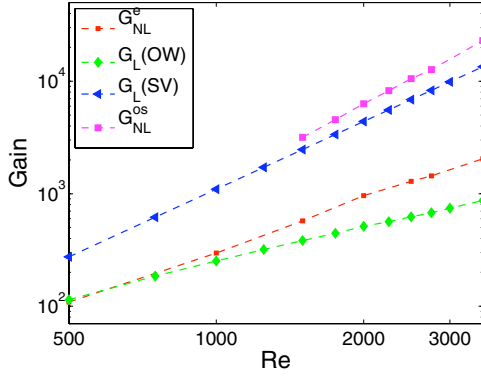$$G_L = \frac{E(t=t_{\max})}{E(t=0)}. \qquad (35)$$

FIG. 12. (Color online) Nonlinear gain G_{NL}^e for the pure oblique-wave initial condition as a function of the Reynolds number Re, compared to the linearly optimal gain G_L for oblique waves [mode $(1, \pm 1)$] and streamwise vortices [mode $(0,2)$]. G_{NL}^{os} is the nonlinear gain including the overshoot before the edge state is reached. See text for the definition of G_{NL}^e and G_{NL}^{os}.

G_L represents the linear transient growth for a given initial disturbance, and it is a linear concept. Now taking nonlinearity into account, G_{NL}^e is the energy gain which has to be achieved in practice to reach the edge state, and later turbulence. Maximizing either G_L or G_{NL}^e over all initial conditions corresponds, respectively, to finding *linear* or *nonlinear* optimal perturbations [see Eq. (17) for the linear case]. The energy of the edge state is chosen as the energy of the first steady state reached from a given initial perturbation, i.e., $E1$ in the OW case ($E2$ or $E3$ in the SV case). In Fig. 12, we have plotted G_{NL}^e for varying Re in the pure OW case, and compared it to the linear gain G_L for both the $(1, \pm 1)$ and the $(0,2)$ modes. As Re $\to \infty$, the ratio G_{NL}^e/G_L increases when considering the $(1, \pm 1)$ modes, while it vanishes for the $(0,2)$ mode. A possible explanation is as follows: when the initial perturbation consists of pure oblique waves, linear growth mechanisms do not extract enough energy from the base flow to bring the perturbation to the energy level $O(E_\Sigma)$, i.e., $G_L(\text{OW})E_0 \ll O(E_\Sigma)$. The larger Re, the clearer the trend. The fact that linear growth of the oblique waves is not sufficient to reach the edge state is not surprising: it is easily explained by the fact that some of the energy of the initial obliques modes is transferred via nonlinear interaction to streamwise-independent modes. The amount of energy transferred can be amplified afterward by a stronger growth mechanism since $G_L(\text{SV})E_0 \gg O(E_\Sigma)$. However, the linear lift-up mechanism amplifying the energy of the streamwise-independent modes now produces an excess of energy compared to the target energy E_Σ. The interpretation is straightforward: as Re increases, less of the full potential for transient growth of the streamwise vortices is used to reach the edge state, which makes transition more likely to occur. Also, if linear mechanisms dominate the whole transient phase of energy growth, then a substantial part of the energy of the perturbation must later be released in order to approach the neighborhood of the edge state.

We wish to quantify this momentaneous excess of energy, both in the presence of linear and nonlinear effects. In order to do so we introduce a second measure of the nonlinear gain, namely, G_{NL}^{os},

$$G_{NL}^{os} = \frac{\max_{t \leq t_{edge}} E(t)}{E(t=0)}, \qquad (36)$$

which takes into account the full dynamics before the edge state is approached. Note that the superscript "os" in "G_{NL}^{os}" stands for "overshoot." G_{NL}^{os} is the maximum nonlinear amplification of energy before the edge state is reached. We always notice an overshoot of the energy preceding the approach to the steady state (see Fig. 2 and 6), hence G_{NL}^{os} is not equal to G_{NL}^e. Furthermore the magnitude of this overshoot is seen to increase monotonically with Re. This is verified in Fig. 12, which shows that the ratio G_{NL}^{os}/G_L is constantly greater than unity no matter whereas G_L is computed for the modes $(1, \pm 1)$ or $(0,2)$. It seems to slowly diverge as $O(\text{Re}^{0.5})$ in the latter case. The instantaneous nonlinear gain G_{NL}^{os} thus exceeds the linear gain of the modes $(0,2)$ and $(1, \pm 1)$, and this trend increases with Re.

While the quantity G_{NL}^e yields only limited information on how nonlinearity affects the transient phase, the alternative measure G_{NL}^{os} has the advantage of pointing out to which extent nonlinear mechanisms elicit larger linear amplification. The larger the value of Re, the stronger the enhancement by nonlinear effects. This behavior is expected to be related to the nonlinear feedback of the growing perturbations on the mean flow [6].

VI. CONCLUSIONS

This investigation is a first step toward the identification of minimal perturbations in subcritical shear flows. The numerical approach is fully nonlinear but makes use of the concept of linear optimal modes, together with the evidence that nonlinear equilibria play a key role for the dynamics near the threshold. We have implemented an optimization algorithm to find minima of the initial energy at the threshold for transition, in a reduced space spanned by linear optimal modes. The threshold energy of a given initial disturbance is identified numerically by the bisection process used to track the edge state of the system. The method was tested in a small periodic cell of plane Couette flow of size $4\pi h \times 2h \times 2\pi h$. It is also applicable for other flows allowing by-pass transition, independently of the nature of the edge state (steady state or chaotic tangle).

In the case of plane Couette flow at Re=400, we have shown how the threshold energy E_c can be decreased by considering initial disturbances with less and less symmetries. For instance, streamwise vortices (SV) are two-dimensional and cannot trigger transition. A pair of oblique modes with equal amplitude (OW) is optimal in the context of bimodal initial disturbances, a fact already referred to in Refs. [28,31]. Note however the turbulent flow reached after transition by pure oblique waves evolves in a restricted symmetry subspace of the system. In the context of trimodal initial disturbances, we have shown the existence of a disturbance M with lower threshold energy than oblique waves, leading to a turbulent flow with broadband spectrum. This state M consists of a pair of oblique modes with nonequal amplitudes, and a third mode $(1,2)$ with a phase shift breaking the oblique symmetry. Spectral analysis of the transition

scenario has demonstrated that the addition of other modes to the oblique pair is the key to an improvement of the initial threshold energy: the additional modes need to be oblique, low-order (weakly damped), and generate nonlinearly substantial spectral components of the edge state, other than (0,2). Note that pure oblique waves interact nonlinearly to produce precisely the streak mode (0,2), which is the linear optimal mode but is above all the dominant spectral component of the edge state. One can hence see the $m=3$ optimization as a multimodal generalization of the pure oblique-wave mechanism, and speculate that adding more modes to the optimization procedure may result in a further decrease of the initial energy. Yet the improvement obtained by going from $m=2$ to $m=3$ is relatively weak ($<2\%$ in energy), so we mainly expect any further improvement to be marginal, because high-order modes are damped on a faster time scale.

This study has also shown shed some light on the role of the steady state solution (called here $E1$), apparently connected to the hairpin vortex solution of Refs. [30,29]. This finite-amplitude state sits on the laminar-turbulent boundary Σ. It plays a crucial role along optimal transition paths since it is the one approached by optimal trajectories starting from either the state M or from pure oblique waves. Compared to other edge states, this one has an additional oblique symmetry, lower energy and lower-amplitudes streaks, with a wide nearly laminar region between the streaks.

We have revisited initial energy thresholds as a function of Re for the two classical SV and OW scenarios, using well-resolved computations. Correcting the results in Ref. [28], we have found a scaling $E_c=O(\text{Re}^{-2})$ for both scenarios, with the energy for the OW scenario constantly one decade below that of the SV scenario. This scaling is in perfect agreement with analytical predictions from Refs. [31,32] and recent experimental suggestions in pipe flow [33].

The optimization method suggested here, based on an expansion on a finite number of linear optimal modes, extends naturally to other shear flows (such as pipe and channels) when few low-order Fourier modes are enough to describe the main large-scale structures. A generalization of this method is desired if spatiotemporal intermittency effects are to be taken into account, for instance if transition occurs through the growth of turbulent spots. In that case other optimization methods, among which adjoint-based algorithms, can also be useful [6]. Our results nevertheless point out that *local* streak breakdown can be enhanced most optimally by oblique waves, which is a useful starting point for any kind of optimization method based on an initial guess.

ACKNOWLEDGMENTS

[1] P. J. Schmid and D. S. Henningson, *Stability and Transition in Shear Flows* (Springer, New York, 2001).

[2] K. Butler and B. F. Farell, Phys. Fluids A **4**, 1637 (1992).

[3] S. C. Reddy and D. S. Henningson, J. Fluid Mech. **252**, 209 (1993).

[4] J. Hœpffner, L. Brandt, and D. S. Henningson, J. Fluid Mech. **537**, 91 (2005).

[5] C. Cossu, M. P. Chevalier, and D. S. Henningson, Phys. Fluids **19**, 058107 (2007).

[6] D. Biau and A. Bottaro, Philos. Trans. R. Soc. London, Ser. A **367**, 529 (2009).

[7] B. Hof, J. Westerweel, T. M. Schneider, and B. Eckhardt, Nature (London) **443**, 59 (2006).

[8] T. M. Schneider, F. De Lillo, J. Buehrle, B. Eckhardt, T. Dörnemann, K. Dörnemann, and B. Freusleben, Phys. Rev. E **81**, 015301(R) (2010).

[9] T. M. Schneider, B. Eckhardt, and J. A. Yorke, Phys. Rev. Lett. **99**, 034502 (2007).

[10] J. Wang, J. Gibson, and F. Waleffe, Phys. Rev. Lett. **98**, 204501 (2007).

[11] T. M. Schneider, J. F. Gibson, M. Lagha, F. De Lillo, and B. Eckhardt, Phys. Rev. E **78**, 037301 (2008).

[12] M. Nagata, J. Fluid Mech. **217**, 519 (1990).

[13] G. Kawahara, Phys. Fluids **17**, 041702 (2005).

[14] H. Faisst and B. Eckhardt, Phys. Rev. Lett. **91**, 224502 (2003).

[15] H. Wedin and R. R. Kerswell, J. Fluid Mech. **508**, 333 (2004).

[16] Y. Duguet, A. P. Willis, and R. R. Kerswell, J. Fluid Mech. **613**, 255 (2008).

[17] Y. Duguet, C. C. T. Pringle, and R. R. Kerswell, Phys. Fluids **20**, 114102 (2008).

[18] F. Waleffe, Phys. Rev. Lett. **81**, 4140 (1998).

[19] F. Waleffe, J. Fluid Mech. **435**, 93 (2001).

[20] S. Toh and T. Itano, J. Fluid Mech. **481**, 67 (2003).

[21] D. Viswanath and P. Cvitanović, J. Fluid Mech. **627**, 215 (2009).

[22] S. C. Reddy and D. S. Henningson, Phys. Fluids **6**, 1396 (1994).

[23] F. Waleffe, Phys. Fluids **7**, 3060 (1995).

[24] D. S. Henningson, Phys. Fluids **8**, 2257 (1996).

[25] C. Cossu, C. R. Mec. **333**, 331 (2005).

[26] M. Chevalier, P. Schlatter, A. Lundbladh, and D. S. Henningson, SIMSON—A Pseudo-spectral Solver for Incompressible Boundary Layer Flows, KTH Mechanics, Stockholm, Sweden, TRITA-MEK 2007:07, 2007.

[27] P. J. Schmid and D. S. Henningson, Phys. Fluids **4**, 1986 (1992).

[28] S. C. Reddy, P. J. Schmid, J. S. Baggett, and D. S. Henningson, J. Fluid Mech. **365**, 269 (1998).

[29] J. F. Gibson, J. Halcrow, and P. Cvitanović, J. Fluid Mech. **638**, 243 (2009).

[30] T. Itano and S. C. Generalis, Phys. Rev. Lett. **102**, 114501 (2009).

[31] J. S. Chapman, J. Fluid Mech. **451**, 35 (2002).

[32] F. Waleffe and J. Wang, *Transition Threshold and the Self-Sustaining Process*, IUTAM Symposium on Laminar-Turbulent Transition and Finite Amplitude Solutions (Springer, Dordecht, 2005).

[33] B. Hof, A. Juel, and T. Mullin, Phys. Rev. Lett. **91**, 244502 (2003).